Mustansiriyah Journal of Pure and Applied Sciences, Print ISSN: 2957-9910. Online ISSN: 2957-9929, Vol. 2, No. 4, 2024, Pages 93-103
DOI:

MJPAS

MUSTANSIRIYAH JOURNAL OF PURE AND APPLIED SCIENCES

Journal homepage*:*
https://mjpas.uomustansiriyah.edu.iq/index.php/mjpas

RESEARCH ARTICLE - PHYSICS

Non-thermal atmospheric jet plasma effects on the morphological, electrical, and optical properties of nanocrystalline silicon

[1]Noor D. Hayif, [2*] Intesar H. Hashim, [3]Hasan A. Hadi
[1] Polymer Research Unit, College of Science, Mustansiriyah University, Baghdad-Iraq
[2] Department of Physics, College of Education, Mustansiriyah University, Baghdad-Iraq
* Corresponding author Email: dr.intesarhato@uomustansiriyah.edu.iq

Article Info. **Abstract**

Article history:

Received
04 December 2023

Accepted
31 March 2024

Publishing
30 September 2024

In this study, a non-thermal atmospheric argon plasma jet NTAPJ was designed and used to treat the porous silicon layer, prepared by photo electrochemical etching PECE. N-type porous silicon layers were distinguished before and after the cold plasma treatment utilized by X-ray diffraction XRD, atomic force microscopy AFM, field emission scanning electron microscopy FE-SEM, photoluminescence PL, and dark and photo current-voltage characteristics. The results confirmed the nanostructure of the formed porous silicon. After the treatment with argon plasma, the intensity of the XRD peak increased, and the porosity decreased from 93% to 62%. Additionally, porous silicon's average roughness Sa and root mean square Sq were reduced from 60.10 to 12.31nm and 73.70 to 16.53nm, respectively. The current-voltage characteristic indicated the increase in photocurrent and the ideality factor, as well as a decrease in dynamic resistance. The photoluminescence results showed a change in PL peaks, represented by a blue shift, an increase in intensity, and a vanishing of another peak.

The official journal published by the College of Education at Mustansiriyah University

Keyword: porous silicon; PECE; NTPAJ; FE-SEM; PL; XRD.

Introduction

In the past few decades, the production of nanomaterials has become an exciting field for researchers because of their unique physical properties that differ from those of crystalline semiconductors[1]. Specifically, porous semiconductor materials, known for their distinct physical, chemical, optical, and biological properties, have received considerable attention in scientific and applied fields [2], [3] . Among the porous materials, porous silicon (PSi) is known as solid silicon with voids that provide a large surface area (200 to 800 $m^2 . g^{-1}$) [2], [3], nano-scale pores [4], and a combination of three-dimensional semiconductor substrates with nanomaterials deposited on them, as well as a surface texture that acts as a light trap, enhancing light absorption in long wavelengths. All of these features have made it favourable for numerous applications, such as optoelectronics [5], [6], [7] biomedical [8], [9], chemical and biosensors [10], [11] and microelectronics [12]. Since the discovery of porous silicon in 1956, over 20 methods have been developed to synthesize porous silicon structures. However, only a few of these methods have gained significant attention. Out of these methods, electrochemical etching is the most widely used [13], [14], [15], [16]. It is both cost-competitive and versatile, allowing for the production of various porous structures with exceptional physical and chemical properties. By adjusting the formation parameters, such as current density, solution composition, and porous silicon etching time, a wide range of porosities and morphologies can be achieved [12], [17], [18].

Porous silicon characteristics could be improved, leading to widened applications by surface modification, which can be achieved by various methods, including chemical processes [19], annealing [20], [21], oxidation [22], as well as plasma treatment [23], [24], [25], [26]. Plasma, composed of electrons, ions, and neutral particles, is a quasi-neutral substance that can be partially or fully ionized. Thermal and non-thermal plasma are two classifications of plasma based on their component temperature, each with distinct characteristics and uses [27]. Various methods, such as plasma jet, dielectric barrier discharge, corona discharge, and arc discharge, can generate cold plasma [28], [29], [30], [31], [32], [33], [34], [35], [36], [37]. Commonly used gases include air, nitrogen, hydrogen, and argon [31], [33], [35], [37]. Non-thermal atmospheric plasma offers several advantages, including producing stable plasma at atmospheric pressure [38] and eliminating the need for a vacuum. It is also economically advantageous due to its simplicity and cost-effectiveness [37]. Additionally, non-thermal atmospheric plasma does not cause thermal damage to treated substrates [35], [38]. This type of plasma has become an essential tool in surface modification, particle deposition, sterilization of medical instruments, and various other applications in fields like biomedical [39], insulation [40], super-wetting surfaces [41], plasma green and eco-friendly [42]. This study aims to examine how non-thermal plasma interacts with the structure of porous silicon, explicitly analyzing its impact on morphological and photoluminescence properties.

Experimental

Photo electrochemical etching cell

Porous silicon layers were fabricated by using the photoelectrochemical method on a n-type Si (111) substrate with a thickness of 200 µm and a resistivity of 0.001 Ω.cm. This was obtained by following a simple setup, as shown in Fig.1, and with the assistance of a halogen lamp. The substrate was cut into 1×1 cm^2 samples, which were then thoroughly cleaned using an ultrasonic device with ethanol, acetone, and distilled water and dried with hot air. The samples were then etched for 15 minutes at a current density of 35 mA/cm^2, using a solution consisting of 40% HF and 99.98% ethanol mixture with a volume ratio 1:3.

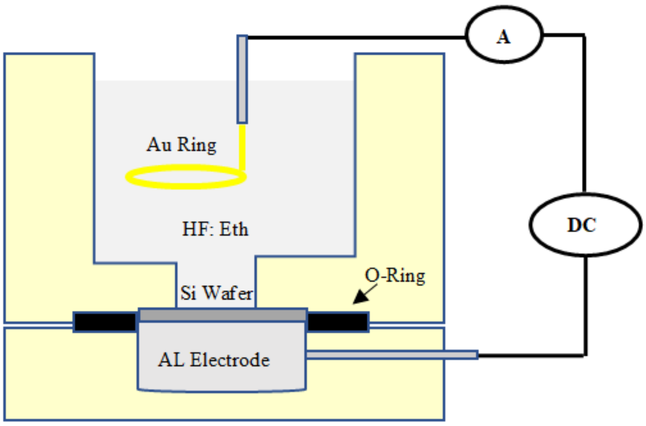

Fig. 1: Electrochemical etching cell

The porous silicon layer's structure was analyzed using x-ray diffraction with PANalytical Aeris X-ray diffractometer (Cu Kα1 radiation and wavelength of 1.54059 Å). The topography of the porous silicon surface was studied using (TT-2 AFM). Additionally, the porous silicon's morphology, thickness, and porosity were examined before and after non-thermal plasma treatment using FE-SEM (Inspect TM F50). To determine the photo luminance peak (optical energy gap), a FluoroMateFS-2 spectrometer was employed.

Non-thermal plasma setup

Fig. 2 shows the designed jet consisting of two coaxial electrodes with dielectric materials, typically Teflon, positioned between them. A 20 kV AC voltage is connected to these electrodes. The inner electrode is a copper tube with a diameter of 1.5mm. In comparison, the outer electrode is a 1 cm long copper cylinder surrounding a glass tube with an inner diameter of 4mm. Argon gas flows at a rate of 10L/min within the copper tube. The plasma is generated between the electrodes and then emitted through the nozzle at the end of the glass tube onto the treatment material. Optical characterization of the discharge was done using Stark broadening and Boltzmann plot methods by analyzing the spectrum obtained using the optical emission spectrometer (HR4000CG-UV-NIR, Ocean Optics); the temperature of the electrons was estimated [43], [44], [45] and was found to be 0.547 eV.

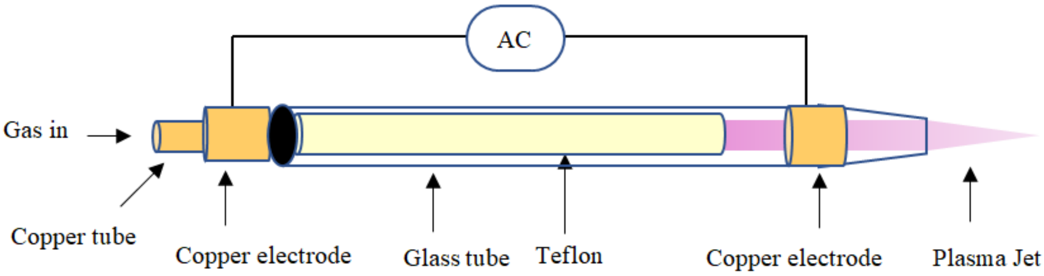

Fig. 2: Schematic of plasma jet

The samples were placed at a distance of 7mm from the jet nozzle, and the treatment operation lasted for ten minutes.

Results and discussion

Fig. 3 displays porous silicon's X-ray diffraction (XRD) patterns before and after argon plasma treatment. Before treatment, the samples exhibited the (111) peak at approximately $2\theta = 28.39$. After argon plasma treatment, an increase in the intensity of the (111) peak was observed, along with a slight shift towards higher angles compared to untreated porous silicon. In addition, there was an increase in the crystalline size (L) and a decrease in the average discrepancy (D%), as calculated using Debye-Scherrer and average discrepancy equations (Eq.1 and Eq.2) [46].

$$L = \frac{K\lambda}{FWHM * \cos\theta} \qquad (1)$$

where L: is crystalline size of porous silicon, FWHM is the full width at half maximum of the diffraction peak, θ is the diffraction angle and λ is the wavelength of the Cu-K-α1line.

$$D\% = \frac{a_{si-}a_{PSi}}{a_{PSi}} \times 100\% \qquad (2)$$

where D: is the lattice parameter variation between the bulk silicon constant a_{Si} and the porous silicon constant a_{PSi} The full width at half maximum (FWHM) was also reduced, indicating an increase in crystalline size. These results are presented in Table 1.

Table 1: XRD result of untreated PSi and treated Psi.

Parameters	Untreated Psi	Treated Psi
L (nm)	81.6 nm	288 nm
The average discrepancy D%	0.0193	0.0053
FWHM (deg.)	0.1299	0.066

For the argon plasma-treated samples, the increase in intensity and decrease in FWHM can be explained by the improvement in the crystalline structure resulting from the formation of uniform pores [47]. The strain induced by surface forces increases as the internal surface area enlarges, closely related to the porous silicon microstructure. The peak shift can be attributed to the strain, and the reduction in micro-strain can be attributed to lattice relaxation caused by changes in the surface microstructure, i.e., the size and shape of the porous silicon [20]. All of these results can be attributed to the plasma's energy rearranging the surface structure of porous silicon.

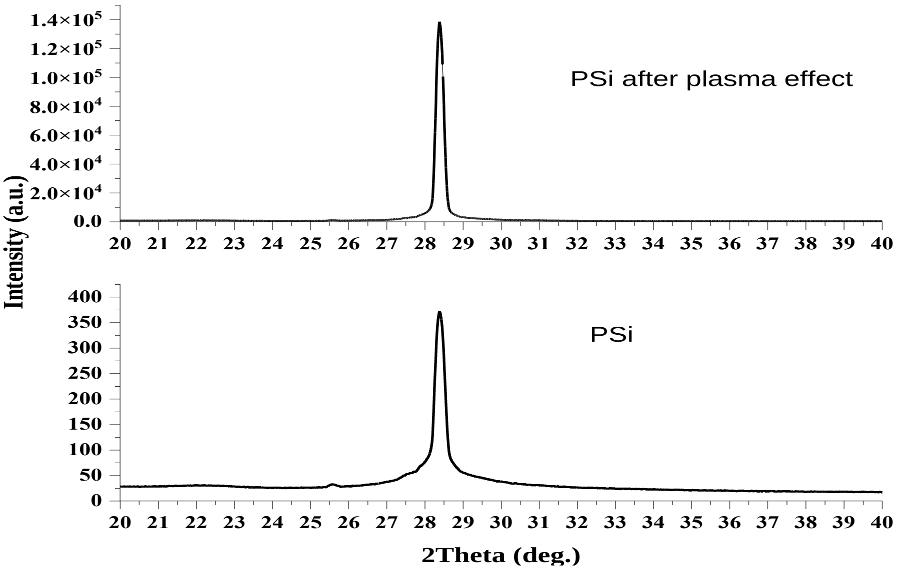

Fig. 3: XRD pattern of porous silicon layer before and after plasma treatment

The FE-SEM images of the porous silicon layer before and after argon plasma treatment (represented by figures 4 a, b, c, and d, respectively) clearly show differences in morphology. The untreated sample exhibits a semi-homogenized structure with small pentagonal and quadrangular holes forming a network. However, after plasma treatment, the walls of the pores become thicker, and the holes change their shape to nearly circular [25].

It has been observed that when porous silicon is treated with cold plasma, its porosity decreases significantly more than that of crystalline silicon that has not been treated. The plasma's energetic ions interact with the porous silicon surface to change its structural composition.

FE-SEM IMGE determined that the untreated sample's porosity was 93%, while after argon plasma treatment, the porosity decreased to 64%.

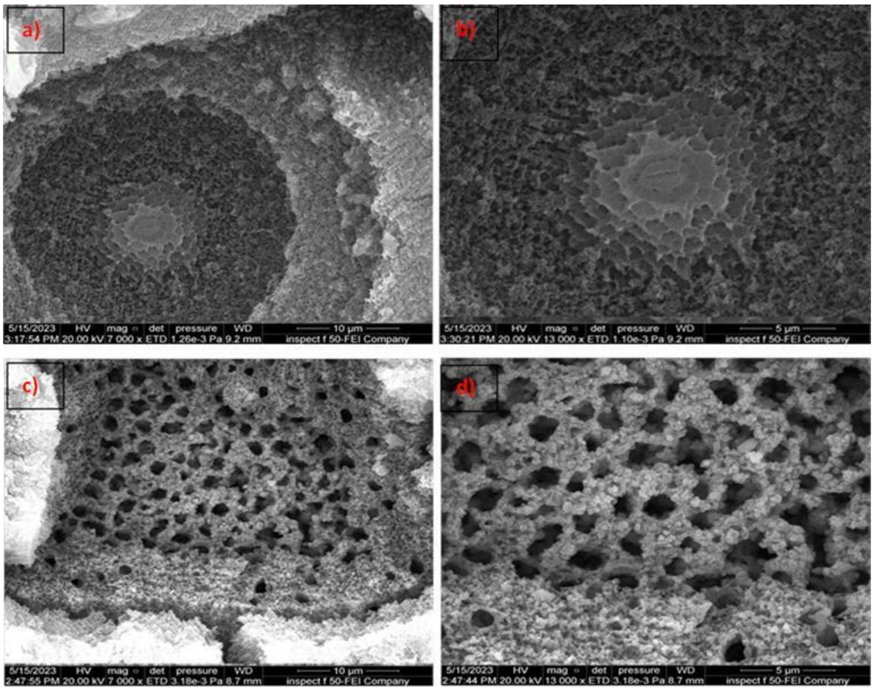

Fig. 4: FE-SEM images of a, b) As grown c, d) Plasma jet treatment of Psi

The 3D images of the porous silicon layer profile (a) and porous silicon following cold plasma treatment (b) are displayed in Figure 5. It is evident that following treatment, the semi-uniformity of pyramidal forms and surface roughness were reduced. The rearrangement and creation of pores on the surface are responsible for this roughness decrease. The amplitude reporting parameters of the samples after non-thermal plasma treatment are presented in Table 2.

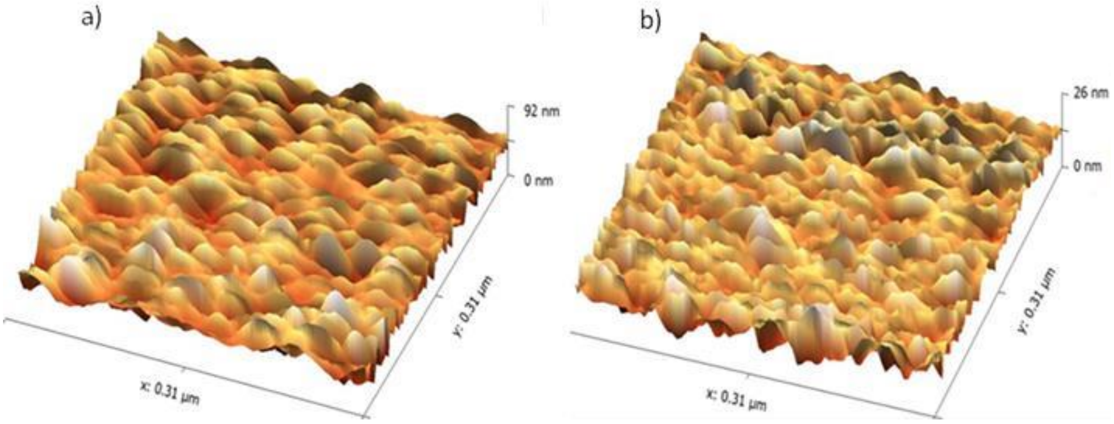

Fig. 5: 3D AFM image of porous silicon a) before and b) after treatment.

Table 2: Roughness Report parameters of fresh PSi and PSi treated.

Amplitude parameters	Fresh Psi	PSi /treatment
Minimum	0.0	0.0
Maximum	108.2 nm	39.93 nm
(Ten Point Height) Sz	461.4 nm	106.4 nm
(Roughness Average) Sa	60.10 nm	12.31 nm
(Root Mean Square) Sq	73.70 nm	16.52 nm

Fig. 6 displays the photoluminescence (PL) spectra of untreated and argon plasma-treated porous silicon at 320 nm wavelength, revealing that the PL peaks range from 560 to 680 nm for untreated porous silicon and from 520 to 645 nm for treated porous silicon. After treatment with argon plasma, specific peaks exhibited an increase in intensity and a shift towards shorter wavelengths (blue shift), as displayed at 647 and 518 nm, and some peaks vanished, as shown at 459 nm. The shift in peak position can be attributed to the luminescence mechanism of quantum confinement [48]. There are two possible reasons for the increase in intensity. One is the presence of SiH_2 in porous silicon and the introduction of oxygen through plasma treatment; this leads to the formation of chemical species that encourage the radiative recombination of electron-hole pairs, increasing light emission. Another possibility is that plasma will fluorinate the surface, which promotes radiative recombination and light emission [23], [26]

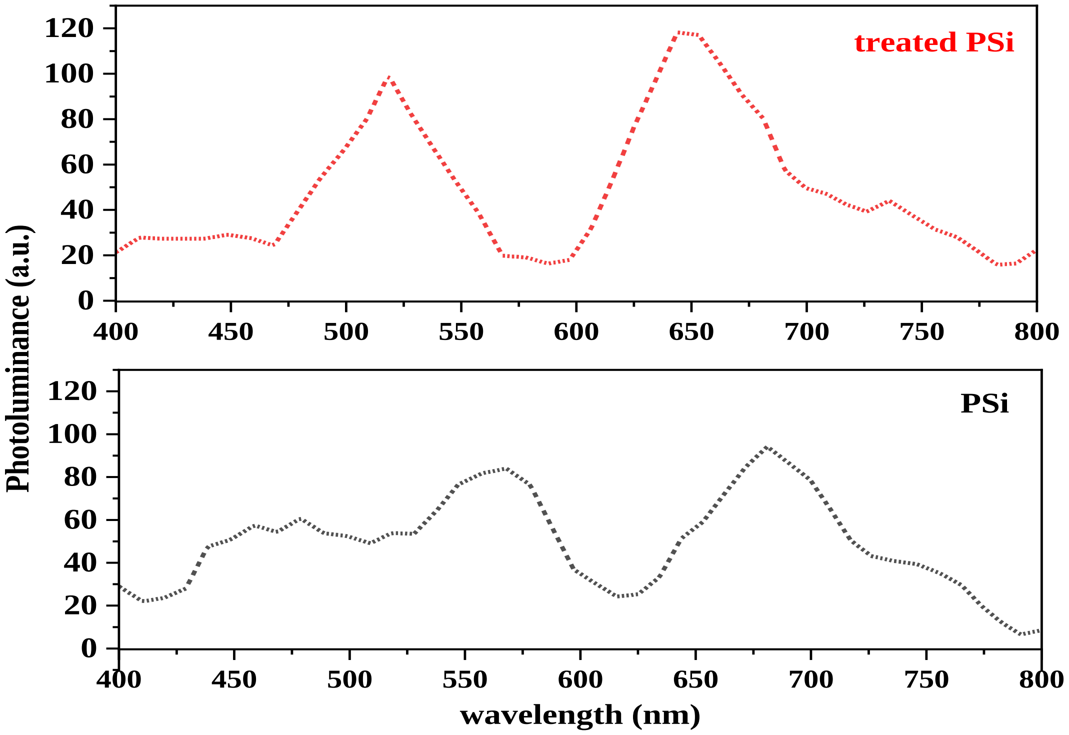

Fig. 6: Photoluminance spectra of porous silicon before (black line) and after (red line) treatment with atmospheric Argon plasma.

The refractive index before and after plasma treatment was calculated using the following [49]:

$$n = \sqrt{\varepsilon_{PSi}} \qquad (3)$$

$$\varepsilon_{PSi} = \varepsilon_{Si} - P\%(\varepsilon_{Si} - 1) \qquad (4)$$

where ε_{PSi}: is the relative permittivity of porous silicon and equal 11.68, ε_{Si}: is the relative permittivity of bulk silicon (equal 1), and P(%): is the porosity

After plasma treatment, calculations revealed an increased refractive index of 1.32 to 2.24, so this technique may be employed to modify the optical characteristics of the porous silicon surface.

Fig. 7 shows the current -voltage characteristic for Psi/n-Si in a semi- log plot, in dark and under illumination (halogen lamp) from -8 to +8 Volts for fresh and argon plasma-treated porous silicon. The result indicated an increase in photocurrent for the non-thermal plasma treated sample, which may be attributed to enhancement in junction structure resulting from a reduction in defect at the Psi/n-Si interface, which means a decrease in the strain. The diode parameters (ideality factor n, barrier height $\emptyset_b$) were calculated using the thermionic emission model equation; the relation between (I-V) is given by [50];

$$\mathrm{I} = \mathrm{I_s}\left[\exp\left(\frac{\mathrm{qV}}{\mathrm{nkT}}\right) - 1\right] \qquad (5)$$

where q electronic charge, T absolute temperature in Kelvin, k Boltzmann constant, V is applied voltage, $\mathrm{I_s}$ the reverse saturation current is calculated from the ln I vs V plot by extrapolating the linear region of the curve to zero applied voltage axis as shown in Fig. 8

$$\mathrm{I}_s = \mathrm{AA^*T^2}\exp\left(\frac{-\mathrm{q}\,\emptyset_b}{\mathrm{nkT}}\right) \qquad (6)$$

$$\emptyset_b = \frac{\mathrm{kT}}{\mathrm{q}}\ln\left(\mathrm{AA^*}\frac{\mathrm{T^2}}{\mathrm{I_s}}\right) \qquad (7)$$

Where A is the area of the diode, A^* is the modified Richardson constant which equal to 112 A cm^{-2} K^{-2} for n-Si, the ideality factor is calculated from current – voltage characteristic by using the following Eq. [51]:

$$n = \frac{q}{KT}\left(\frac{dV}{d\ln I}\right. \qquad (8)$$

The resistance R_d is calculated from the linear part of the forward bias (I-V) plot and the rectification ratio RR is calculated from the ratio between the forward to reverse current. The result obtained from the analysis of the (I-V) characteristic is summarized in Table 3.

Table 3: (I-V) characteristic of fresh PSi and PSi treated.

Parameters	Untreated Psi	Treated Psi
I_s	5.25×10^{-7}	6.14×10^{-6}
n	2.4	2.6
ϕ_b	0.758	0.683
R_d	167 kΩ	100 kΩ
RR	4	33

The results indicated that after argon plasma treatment, there is an increase in reverse saturation current accompanied by a decrease in the barrier height and a decrease in resistance, which may be attributed to the reduction in layer thickness and porosity. A non-homogeneously porous silicon layer may lead to a high ideality factor of more than one, and the increase in ideality factor may be caused by the surface oxidation of porous silicon after non-thermal plasma treatment.

The increased photo-current can be attributed to several factors. Firstly, cold plasma treatment can enhance the surface passivation of porous silicon, and secondly, modify the surface properties of porous silicon, leading to changes in its electrical behaviour and reducing the surface recombination of photo-generated carriers. This reduction in carrier recombination improves the overall efficiency of the material, leading to higher photo-current generation.

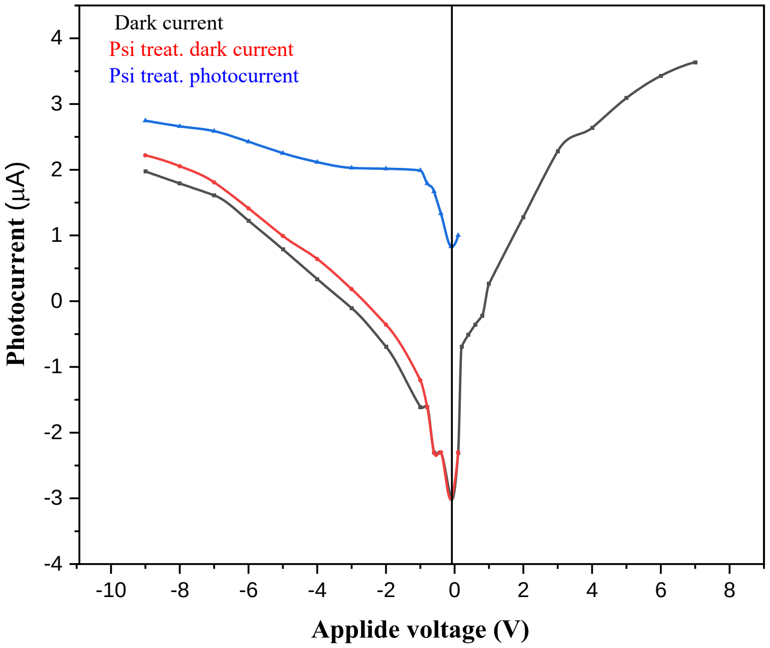

Fig. 7: Photocurrent of PSi/n-Si diode before (red line) and after (blue line) plasma treatment.

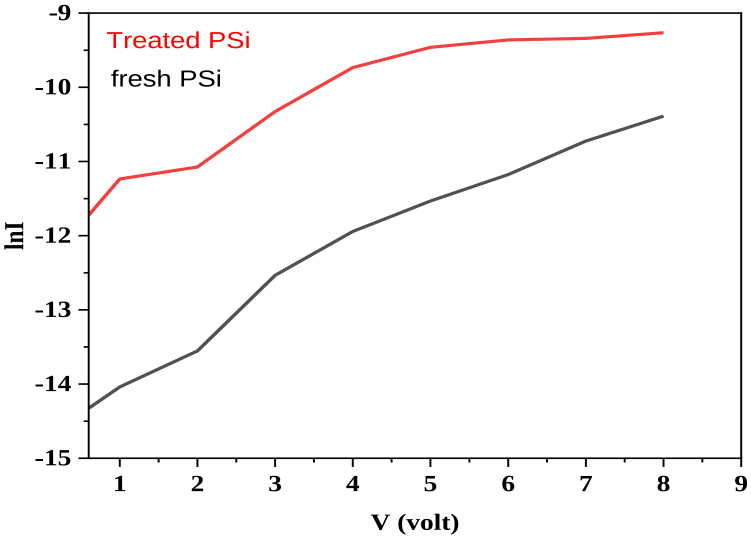

Fig. 8: lnI versus voltage

Conclusions

This study investigated the impact of jet plasma on the morphological, electrical, and optical properties of nanocrystalline porous silicon. The photoelectrochemical etching method was used to fabricate a porous silicon layer.

The n-type porous silicon surface was effectively created, and its microstructure, morphological, and electrical properties were compared to those of the untreated surface.The surface of porous silicon can be passivity by non-thermal plasma by forming a barrier. The electrical characteristics of porous silicon devices, like solar cells or sensors, can be improved, and this passivation layer can decrease surface recombination. It contributes to increased device stability and efficiency.Low-temperature plasma treatment is beneficial because it maintains the material's structural integrity and porosity, which are essential for its special qualities and uses. Treating the PSi surface with cold plasma could further improve the morphological, optical, electrical, and optoelectronic capabilities of the porous silicon layer, it contributes to increased device stability and efficiency.Modifying and treating nanostructures of porous silicon using non-thermal jet plasma technologies are very promising.

Acknowledgments

The study was conducted at the Thin Films Laboratory in the College of Education, Department of Physics at Mustansiriyah University. The authors would like to express their gratitude to Mustansiriyah University, Baghdad, Iraq, for providing logistical support during the research.

References

[1] N. A. Abdulkhaleq, A. K. Hasan, and U. M. Nayef, “Enhancement of photodetectors devices for silicon nanostructure from study effect of etching time by photoelectrochemical etching Technique,” *Optik (Stuttg).*, vol. 206, pp. 164325, 2020.

[2] and V. U. E. Monaico, I. Tiginyanu, “Porous semiconductor compounds,” *Semicond. Sci. Technol.*, vol. 35, no. 10, pp. 103001, 2020.

[3] E. Xifré-Pérez, J. Ferré-Borrull, J. Pallarés, and L. F. Marsal, “Methods, properties and applications of porous silicon,” *Electrochem. Eng. Nanoporous Mater. Methods, Prop. Appl.*, pp. 37–63, 2015.

[4] S. Arshavsky-Graham, S. J. Ward, N. Massad-Ivanir, T. Scheper, S. M. Weiss, and E. Segal, “Porous silicon-based aptasensors: toward cancer protein biomarker detection,” *ACS Meas. Sci. Au*, vol. 1, no. 2, pp. 82–94, 2021.

[5] H. A. Hadi, R. A. Ismail, and N. F. Habubi, “Optoelectronic properties of porous silicon heterojunction photodetector,” *Indian J. Phys.*, vol. 88, pp. 59–63, 2014.

[6] H. A. Hadi and R. A. Ismail, “Preparation and Characteristics Study of High-Quantum Efficiency Ni/PSi/c-Si and cd/PSi/c-Si Double-Junction Photodetectors,” *Silicon*, vol. 14, no. 17, pp. 11089–

11096, 2022.

[7] S. T. Kassim, H. A. Hadi, and R. A. Ismail, "Fabrication and characterization of high photosensitivity CuS/porous silicon heterojunction photodetector," *Optik (Stuttg).*, vol. 221, pp. 165339, 2020.

[8] E. Secret *et al.*, "Antibody-functionalized porous silicon nanoparticles for vectorization of hydrophobic drugs," *Adv. Healthc. Mater.*, vol. 2, no. 5, pp. 718–727, 2013.

[9] D. Liu, M.-A. Shahbazi, L. M. Bimbo, J. Hirvonen, and H. A. Santos, "Biocompatibility of porous silicon for biomedical applications," in *Porous silicon for biomedical applications*, Elsevier, pp. 129–181, 2014.

[10] F. A. Harraz, "Porous silicon chemical sensors and biosensors: A review," *Sensors Actuators B Chem.*, vol. 202, pp. 897–912, 2014.

[11] S. Pace, R. B. Vasani, W. Zhao, S. Perrier, and N. H. Voelcker, "Photonic porous silicon as a pH sensor," *Nanoscale Res. Lett.*, vol. 9, pp. 1–7, 2014.

[12] G. C. Tettamanzi, S. J. Hile, M. G. House, M. Fuechsle, S. Rogge, and M. Y. Simmons, "Probing the quantum states of a single atom transistor at microwave frequencies," *ACS Nano*, vol. 11, no. 3, pp. 2444–2451, 2017.

[13] H. A. Hadi, R. A. Ismail, and A. R. Abdulwahhab, "Effect of Gamma Irradiation on the Optoelectronics Properties of Porous Si/c-Si Heterojunction photodetector," *Silicon*, pp. 1–10, 2023.

[14] H. A. Hadi, S. T. Kasim, F. K. Farhan, R. A. Ismail, and N. F. Habubi, "Effect of porosity on thermal properties of porous silicon," *Silicon*, vol. 15, no. 6, pp. 2715–2725, 2023.

[15] H. A. Hadi, "Modification of surface properties of silicon wafers by laser-assisted electrochemical etching," *Int. Lett. Chem. Phys. Astron.*, vol. 80, pp. 30–39, 2018.

[16] O. Bisi, S. Ossicini, and L. Pavesi, "Porous silicon: a quantum sponge structure for silicon based optoelectronics," *Surf. Sci. Rep.*, vol. 38, no. 1–3, pp. 1–126, 2000.

[17] H. A. Hadi, "Fabrication and characterization of Sn/PS/p-Si Photodetector," *J. Coll. Educ. Mustanseriyah Univ.*, vol. 3, 2013.

[18] L. Canham, *Handbook of porous silicon*. Springer International Publishing Berlin, Germany:, 2014.

[19] I. Rathinamala, N. Jeyakumaran, and N. Prithivikumaran, "Influence of HCl Treatement on Porous Silicon for Optoelectronic Applications," *J. Nano. Adv. Mat*, vol. 5, no. 2, pp. 67–74, 2017.

[20] N. Milenkovic, M. Drießen, C. Weiss, and S. Janz, "Porous silicon reorganization: Influence on the structure, surface roughness and strain," *J. Cryst. Growth*, vol. 432, pp. 139–145, 2015.

[21] Y. H. Ogata, N. Yoshimi, R. Yasuda, T. Tsuboi, T. Sakka, and A. Otsuki, "Structural change in p-type porous silicon by thermal annealing," *J. Appl. Phys.*, vol. 90, no. 12, pp. 6487–6492, 2001.

[22] Y. Xiao, M. J. Heben, J. M. McCullough, Y. S. Tsuo, J. I. Pankove, and S. K. Deb, "Enhancement and stabilization of porous silicon photoluminescence by oxygen incorporation with a remote-plasma treatment," *Appl. Phys. Lett.*, vol. 62, no. 10, pp. 1152–1154, 1993.

[23] N. G. Galkin *et al.*, "How plasma preprocessing affects the luminescence properties of porous silicon," *J. Opt. Technol.*, vol. 81, no. 8, pp. 431–434, 2014.

[24] M. Pérez *et al.*, "Effect of ammonia plasma treatment on the luminescence and stability of porous silicon," *Mater. Lett.*, vol. 216, pp. 277–280, 2018.

[25] B. M. Kostishko, A. V Drozdov, P. V Shibaev, and A. E. Kostishko, "Argon-oxygen ion-plasma treatment modifies the surface composition and photoluminescence spectrum of porous silicon," *Tech. Phys. Lett.*, vol. 26, pp. 919–922, 2000.

[26] S. Thomas, M. Mozetic, U. Cvelbar, P. Spatenka, and K. M. Praveen, *Non-thermal plasma technology for polymeric materials: applications in composites, nanostructured materials, and biomedical fields*. Elsevier, 2018.

[27] N. N. Misra, O. Schlüter, and P. J. Cullen, *Cold plasma in food and agriculture: fundamentals and applications*. Academic Press, 2016.

[28] J. Pinson and D. Thiry, *Surface modification of polymers: methods and applications*. John Wiley & Sons, 2020.

[29] S. Dou, L. Tao, R. Wang, S. El Hankari, R. Chen, and S. Wang, "Plasma-assisted synthesis and

surface modification of electrode materials for renewable energy," *Adv. Mater.*, vol. 30, no. 21, pp. 1705850, 2018.

[30] K. Ollegott, P. Wirth, C. Oberste-Beulmann, P. Awakowicz, and M. Muhler, "Fundamental properties and applications of dielectric barrier discharges in plasma-catalytic processes at atmospheric pressure," *Chemie Ing. Tech.*, vol. 92, no. 10, pp. 1542–1558, 2020.

[31] C. Alemán, G. Fabregat, E. Armelin, J. J. Buendía, and J. Llorca, "Plasma surface modification of polymers for sensor applications," *J. Mater. Chem. B*, vol. 6, no. 41, pp. 6515–6533, 2018.

[32] H. D. Stryczewska, "Supply systems of non-thermal plasma reactors. Construction review with examples of applications," *Appl. Sci.*, vol. 10, no. 9, pp. 3242, 2020.

[33] S. K. Pankaj, Z. Wan, and K. M. Keener, "Effects of cold plasma on food quality: A review," *Foods*, vol. 7, no. 1, pp. 4, 2018.

[34] M. Izadjoo, S. Zack, H. Kim, and J. Skiba, "Medical applications of cold atmospheric plasma: State of the science," *J. Wound Care*, vol. 27, no. Sup9, pp. S4–S10, 2018.

[35] R. Mandal, A. Singh, and A. P. Singh, "Recent developments in cold plasma decontamination technology in the food industry," *Trends food Sci. Technol.*, vol. 80, pp. 93–103, 2018.

[36] M. Laroussi, "Plasma medicine: a brief introduction," *Plasma*, vol. 1, no. 1, pp. 47–60, 2018.

[37] U. Cvelbar *et al.*, "White paper on the future of plasma science and technology in plastics and textiles," *Plasma Process. Polym.*, vol. 16, no. 1, pp. 1700228, 2019.

[38] J. Li *et al.*, "Porous silicon nanocarriers boost the immunomodulation of mitochondria-targeted bovine serum albumins on macrophage polarization," *ACS Nano*, vol. 17, no. 2, pp. 1036–1053, 2023.

[39] N. A. Krueger *et al.*, "Porous silicon gradient refractive index micro-optics," *Nano Lett.*, vol. 16, no. 12, pp. 7402–7407, 2016.

[40] D. Li, K. Xu, and Y. Zhang, "A review on research progress in plasma-controlled superwetting surface structure and properties," *Polymers (Basel).*, vol. 14, no. 18, pp. 3759, 2022.

[41] J. Batur *et al.*, "Molecular Modification of Zeolites with Cold Atmospheric-Pressure Plasma Jet: A Green and Facile Strategy," *Chem. Mater.*, vol. 35, no. 10, pp. 3867–3879, 2023.

[42] C. H. Rodríguez, J. de J. P. Bueno, A. X. M. Pérez, M. R. Flores, and G. Oza, "Photoelectrocatalytic activity of silicon nanowires decorated with electroless copper nanoparticles and graphene oxide using a plasma jet for removal of methyl orange under visible light," *RSC Adv.*, vol. 13, no. 16, pp. 10621–10635, 2023.

[43] I. H. Hashim, A. K. L. Oudah, and B. J. Hussein, "Impact of Electrodes Material on the Properties of Atmospheric DBD Plasma," *Iraqi J. Sci.*, pp. 4273–4280, 2023.

[44] R. Q. M. B. M. Ahmed, "Optical Diagnostics of Zn foil using Non thermal plasma jets (NTPJ) via high voltage," *MUSTANSIRIYAH JOURNAL OF PURE AND APPLIED SCIENCES*, vol. 2, no. 2, pp. 112–125, 2024.

[45] B. A. Z. Z. M. Abood and A. A. Khadayeir, "Measurement of Electron temperature (Te) and Electron density (ne) Cold Plasma Jets Optical Emission Spectroscopy (OES) Method," *MUSTANSIRIYAH JOURNAL OF PURE AND APPLIED SCIENCES* , vol. 2, no. 2, pp. 126–133, 2024.

[46] W. L. Bragg, "The diffraction of short electromagnetic rays by a crystal," *Scientia*, vol. 45, pp. 153–162, 1929.

[47] R. Radzali, M. Z. Zakariah, A. Mahmood, A. F. A. Rahim, Z. Hassan, and Y. Yusof, "The effect of ecthing duration on structural properties of porous Si fabricated by a new two-steps alternating current photo-assisted electrochemical etching (ACPEC) technique for MSM photodetector," in *AIP Conference Proceedings*, AIP Publishing, 2017.

[48] T. Wang, X. LIa, W. Feng, W. LId, C. TAOd, and J. WENa, "Structure and photoluminescence properties of the quasi-regular arrangements of porous silicon," *Optoelectron. Adv. Mater. Commun.*, vol. 5, no. May 2011, pp. 495–498, 2011.

[49] F. Parlaktürk, A. Agasiev, A. Tataroğlu, and Ş. Altindal, "Current-voltage (IV) and Capacitance-voltage (CV) characteristics of Au/Bi4Ti3O12/SnO2 structures," *Gazi Univ. J. Sci.*, vol. 20, no. 4, pp. 97–102, 2007.

[50] M. Zhou, Z. Shen, Z. Jia, and X. Wang, "Effect of Plasma on Hydrophobicity Migration of Contaminated HTV Silicone Rubber," in *2023 IEEE 4th International Conference on Electrical Materials and Power Equipment (ICEMPE)*, IEEE, pp. 1–4, 2023.

[51] A. A. M. Farag, “Structure and transport mechanisms of Si/porous Si n–p junctions prepared by liquid phase epitaxy,” *Appl. Surf. Sci.*, vol. 255, no. 6, pp. 3493–3498, 2009.